Journal of
Materials Chemistry A

Accepted Manuscript

This article can be cited before page numbers have been issued, to do this please use: R. Ranjan, A. Prakash, A. Singh, A. Singh, A. Garg and R. K. Gupta, *J. Mater. Chem. A*, 2017, DOI: 10.1039/C7TA09193A.

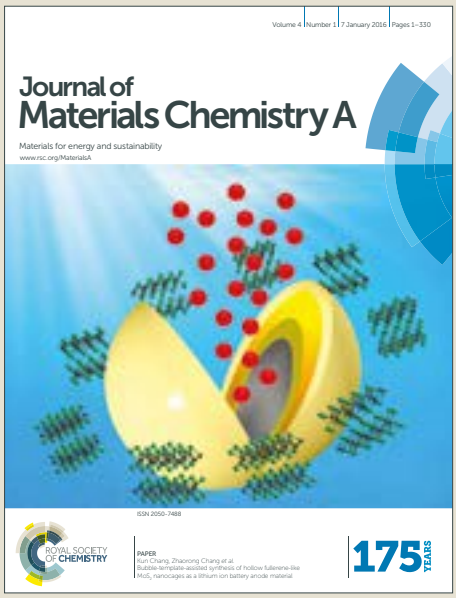

This is an Accepted Manuscript, which has been through the Royal Society of Chemistry peer review process and has been accepted for publication.

Accepted Manuscripts are published online shortly after acceptance, before technical editing, formatting and proof reading. Using this free service, authors can make their results available to the community, in citable form, before we publish the edited article. We will replace this Accepted Manuscript with the edited and formatted Advance Article as soon as it is available.

You can find more information about Accepted Manuscripts in the author guidelines.

Please note that technical editing may introduce minor changes to the text and/or graphics, which may alter content. The journal's standard Terms & Conditions and the ethical guidelines, outlined in our author and reviewer resource centre, still apply. In no event shall the Royal Society of Chemistry be held responsible for any errors or omissions in this Accepted Manuscript or any consequences arising from the use of any information it contains.

ROYAL SOCIETY OF CHEMISTRY

rsc.li/materials-a

Effect of tantalum doping in TiO_2 compact layer on the performance of planar Spiro-OMeTAD free perovskite solar cells

Rahul Ranjan,[†] Asit Prakash,[‡] Arjun Singh,[‡] Anand Singh,*[,§] Ashish Garg,*[,‡] and Raju Kumar Gupta*[,†,‼]

[†]Department of Chemical Engineering

[‡]Department of Materials Science and Engineering

[§]Department of Chemistry

[‼]Center for Nanosciences and Center for Environmental Science and Engineering

Indian Institute of Technology Kanpur, Kanpur 208016, Uttar Pradesh, India

*Corresponding author. Tel: +91-5122596972; Fax: +91-5122590104.

E-mail address: Anand Singh (anands@iitk.ac.in); Ashish Garg (ashishg@iitk.ac.in); Raju Kumar Gupta (guptark@iitk.ac.in)

Abstract

Perovskite solar cells (PSCs) are currently the most exciting solar photovoltaic technologies for future deployment. Conventional PSC device structure typically employs a titanium dioxide (TiO_2) electron transport layer. However, low electrical conductivity of TiO_2 is an obstacle to PSC efficiency enhancement. In this paper, we report on the conductivity enhancement of TiO_2 by tantalum (Ta) doping and its effect on improving the device performance. In contrast to commonly used mesoporous TiO_2, our work used planar PSC device structure based on compact TiO_2 layer with device structure being: FTO/compact-TiO_2/$CH_3NH_3PbI_3$/P3HT/Ag. Photovoltaic measurements show that Ta doping of compact TiO_2 results in an improvement in the fill factor (FF) of the devices due to decrease in the series resistance (R_s), attributed to improved charge transport and increase in the shunt resistance (R_{sh}), due to reduced leakage paths. These changes were examined using Kelvin probe force microscopy (KPFM) which indicated that the Fermi level of TiO_2 shifts downward upon Ta doping providing driving force for the electron transfer from perovskite LUMO to TiO_2 conduction band resulting in higher current density. Further, impedance spectroscopy analysis of the devices suggests a decrease in the charge transfer resistance with Ta-doping and increase in R_{sh} due to higher recombination resistance of doped film. PSC

View Article Online
DOI: 10.1039/C7TA09193A

devices with Ta doping of 3.0% led to a 40% improvement in the overall efficiency as compared to un-doped TiO_2 with best device showing power conversion efficiency of *ca.* 9.94% .

Keywords: Doping, planar perovskite solar cells, compact TiO_2, impedance spectroscopy, Spiro-OMeTAD free perovskite solar cells

1. Introduction

Perovskite solar cells (PSCs) have emerged as an exciting solar photovoltaic technology due to high absorption coefficient of perovskite compounds, high charge-carrier mobility, long exciton diffusion length and a tunable band gap which allows the PSCs to offer a balance between high power conversion efficiency (PCE) and potentially low cost fabrication.[1-6] The reported PCE of the perovskite based solar cells have rapidly increased from 3.9 % in 2009[7] to 22.1% in 2017,[8] indicating significant progress within a short period of time. The most common hole transport layer (HTL) used in regular structure are spiro-OMeTAD (N^2,N^2,$N^{2'}$,$N^{2'}$,N^7,N^7,$N^{7'}$,$N^{7'}$-octakis(4-methoxyphenyl)-9,9′-spirobi[9H-fluorene]-2,2′,7,7′-tetramine), P3HT (poly-3-hexylthiophene) and PTAA (poly(triaryl amine)). To further enhance the conductivity of Spiro-OMeTAD, additives such as Li-TFSI (bis(trifluoromethane)sulfonimide lithium salt) and t-BP (4-*tert*-butylpyridine) are commonly used. Strategies such as use of C60 as electron transport layer with Spiro-OMeTAD have achieved PCE of 19.1% and another group by use of triple cation perovskite and Spiro-OMeTAD as HTL has got PCE of 21.1%.[9-10] Researchers have also sought to replace expensive as well as moisture sensitive hole transporting layer of Spiro-OMeTAD by conjugated polymer P3HT, due to its hydrophobic nature and could prevent moisture from reaching perovskite layer, thus rendering higher atmospheric stability. *Guo et al.* achieved PCE of 12.4% with optimum doping of Li-TFSI and D-TBP (2,6-di-tert-butylpyridine) in P3HT. Although hygroscopic nature of Li and corrosive nature of the pyridine derivative has been found to deteriorate the perovskite, when these additives are used with P3HT, the degradation of perovskite layer is reduced compared to cases in which Spiro-OMeTAD or PTAA are employed.[11]

The emergence of perovskite materials with ambipolar properties has provided the platform for the development of planar heterojunction (PHJ) perovskite solar cells.[12] In PHJ

View Article Online
DOI: 10.1039/C7TA09193A

perovskite, use of mesoporous TiO_2 can be avoided leading to simpler and low thermal budget processing. Here, characteristics of electron transport layer (ETL) are critical to PHJ perovskite solar cell performance due to dual role of ETL as electron transport as well as hole blocking layer. In PHJ PSCs, different metal oxides have been used as ETL. Researchers have used various materials for use as ETL in PHJs such as ZnO, SiO_2, ZrO_2.[13] Liu et al. used thin film of ZnO nanoparticles as an ETL in PSCs and achieved the efficiency of 15.7%.[14] Tseng et al. achieved 15.9% efficiency of PSCs using sputtered ZnO thin film as an ETL having device structure as ITO/ZnO/Perovskite/Spiro-OMeTAD/Ag. It was found that the atmosphere of the sputtering chamber could tune the surface electronic properties (band structure) of the ZnO thin film resulting in improved performance of the PSC.[15] Recently, ultrathin SnO_2 was prepared using atomic layer deposition (ALD) method and was utilized as ETL in PSCs.[16]

TiO_2 has emerged as a promising candidate due to its low cost and high chemical stability and hence is one of the most used ETL for PSCs. Though, the charge transport property such as conductivity of the TiO_2 compact thin film is rather poor and needs to be improved for efficient charge extraction. One of the simple and effective ways to improve the electrical and optical properties of TiO_2 is its chemical doping using an appropriate ion. There are several methods reported for doping in TiO_2 such as Li doping by electrochemical method, yttrium doping using hydrothermal method etc.[17-18] In past, different dopants such as Y, Zn, Mg, Nb have been used in compact as well as mesoporous TiO_2 layer and have resulted in improved electron transport properties of TiO_2 layer; thereby improving the photovoltaic performance of PHJ PSC devices consisting of TiO_2 as ETL (doped or undoped), $CH_3NH_3PbI_{3-x}Cl_x$ as absorber and Spiro-OMeTAD as HTM.[19-24] The improvements have been attributed to better energy level alignment leading to improved electron transport and hole blocking upon Zn doping,[23] positive shift in the flat-band potential and increased conductivity upon Nb doping.[21] Recently, in dye sensitized solar cells (DSSCs), group V element Ta was used to dope TiO_2 (Ta-TiO_2) electron transport layers resulting in an enhanced photovoltaic performance.[25-26] In addition to PCE improvements, there are reports on reduced hysteresis too e.g. in device using Li-doped compact TiO_2 layer.[27]

Among various ions used for doping in TiO_2, Tantalum (Ta) appears as a good choice as Ta^{5+} ion has an ionic radius of 0.64 Å which is comparable to Ti^{4+} (0.61 Å), hence it can substitute Ti^{4+} sites in the TiO_2 framework without issues such as strain or formation of

View Article Online
DOI: 10.1039/C7TA09193A

secondary phases. It is shown to work better than Nb, another group V element [28] and has a negative formation energy and superior thermodynamic stability over N-doped TiO_2.[29] Although Ta doping results in an enhancement in current density of the devices, one study attributed it to positive shift in the flat-band potential[25] while another report showed negligible shift in the flat-band potential.[30] However, most of the works related to doping in TiO_2 are on devices consisting of Spiro-OMeTAD as HTL while TiO_2 has been used in mesoporous structure. Therefore, there is a need to understand the role of Ta doping in compact TiO_2 layers on PSC device performance along with the use of cheaper and environmentally stable HTLs i.e. P3HT. Also, there exists a trade-off between time and efficiency when one uses planar structure with P3HT as HTL. In this manuscript, we present our results on compact Ta doped TiO_2 (Ta-TiO_2) layer as an ETL in perovskite solar cells in conventional planar perovskite structure of FTO/compact-TiO_2/$CH_3NH_3PbI_3$/P3HT/Ag with device structure incorporating P3HT as HTL instead of routinely used Spiro-OMeTAD. Literature reports various methods for the preparation of TiO_2 film such as sol-gel, ALD, electrochemical deposition and DC-magnetron sputtering.[31] We have used sol-gel method for the preparation of compact TiO_2 layer. Further, we investigated the effect of different Ta-TiO_2 layers with varying stoichiometry (1.0-5.0 mol% doping) on device performance by conducting detailed electrical, optical and morphological characterization e.g. electrical conductivity, absorption spectra, Fermi level and surface morphology. Charge carrier dynamics studies on Ta-TiO_2 thin films using photoluminescence (PL) and KPFM show that a shift in the Fermi level along with improved conductivity of Ta-TiO_2 results in a larger driving force for electron transport and thus enhance the short circuit current and fill factor of the devices rendering a maximum PCE of 9.94%.

2. Experimental Details

2.1 Materials

Methylamine solution (CH_3NH_2, 40 wt% in absolute ethanol), hydroiodic acid (HI, 57% in water), lead acetate (99.999 trace metal basis)($Pb(OAc)_2$), anhydrous dimethylformamide (DMF), poly(3-hexylthiophene-2,5-diyl)(P3HT), tantalum(V) ethoxide, fluorine doped tin oxide (FTO) were purchased from Sigma-Aldrich and were used without further purification.

2.2 Synthesis of methylammonium iodide

Under nitrogen atmosphere, 10 mL HI was added dropwise while stirring to 24 mL methylamine solution in 100 mL of ethanol at room temperature. Methylammonium iodide

View Article Online
DOI: 10.1039/C7TA09193A

(MAI) was obtained by concentrating the reaction mixture in vacuum. The white crystals obtained were washed three times in diethyl ether and dried overnight in a vacuum oven.[32]

2.3 Fabrication of solar cell devices

FTO layer on glass substrates was patterned by etching with Zn powder and 2M HCl followed by cleaning with soap and then ultrasonication in DI water, acetone and isopropyl alcohol respectively for 10 min with nitrogen blow drying after each step. Cleaned substrates were UV-ozone treated for 15 min having pretreatment of UV only for 10 min and post treatment of oxygen only for 10 min. Solution of depositing compact TiO_2 ETL layers was prepared by dissolving Titanium diisopropoxide bis(acetylacetonate) solution in ethanol in 1:9 ratio with mixing of tantalum (V) ethoxide in titanium precursor solution in 1.0, 3.0 and 5.0 mol% for doped films. The solution was spin coated on UV-ozone treated substrates at 3000 rpm for 1 min followed by annealing at 100ºC for 10 min on hot plate and at 500ºC for 30 min in a muffle furnace in air resulting in ~ 40 nm thin compact TiO_2 films. The compact TiO_2 layer coated substrates were transferred to the glove box after cooling to room temperature. For depositing perovskite layers, a solution was prepared by mixing methyl ammonium iodide (CH_3NH_3I) and $Pb(OAc)_2$ with 3:1 ratio in DMF to get a 40 wt% solution which was kept in glove box for 2 h at 70ºC. The filtered perovskite solution was spin coated on TiO_2 coated substrates at 2000 rpm for 1 min followed by bench drying for 5 min leading to the formation of a light brownish film and then kept at 100ºC for 10 min rendering the film to become dark brownish. Thickness of final perovskite film was measured to be *ca*. 250 nm. Subsequently, P3HT solution (20 mg/mL in chlorobenzene) was coated at 2000 rpm for 30 s having thickness of ~ 60 nm, followed by thermal evaporation of an 80 nm thin Ag layer at 0.5 Å/s to form the top electrodes.

2.4 Thin film and device characterization

The conductivity of compact undoped TiO_2 and Ta-TiO_2 films was measured using Keithley 2400 source meter using two probe methods on device structure of FTO/TiO_2/Au. For structure analysis, X-ray diffraction (XRD) of the films was conducted on X'Pert Pro (PANanalytical) diffractometer. Chemical states were examined using X-ray photoelectron spectroscopy (XPS) using PHI 5000 (Versa Probe II, FEI Inc) while XPSPEAK 4.1 software was used for analysing the spectra. Agilent technologies, Cary 7000 spectrophotometer was used for absorbance measurements. Raman spectrometer (WiTec, using laser light of λ = 532 nm) was used for Raman studies. Morphological studies of the films were conducted on Asylum MFP-3D AFM and field emission scanning electron microscope (FESEM, Quanta

200, Zeiss). The surface potential was measured using Kelvin-Probe force microscopy (KPFM) using Asylum MFP-3D AFM. Photovoltaic device characteristics were measured using a Keithley 2400 source meter under dark and simulated solar light (AM1.5G) using a Newport solar simulator. Bruker DektakXT stylus profilometer was used for measuring the film thickness. Photoluminescence (PL) of the samples was measured using Horiba Jobin Yvon Fluorolog-3 spectrofluorometer. External quantum efficiency (EQE) was measured using Newport IQE200 system. Impedance spectroscopy measurements were carried out using Potentiostat/Galvanostat (Autolab 302N, Metrohm, Netherlands).

3. Results and Discussion

Initially, we fabricated a 250 nm perovskite thin film on FTO/TiO_2 substrate to study the formation of perovskite film and its grain structure. Fig. S1 shows XRD pattern, absorbance data and morphology of the perovskite film. The film exhibited a single perovskite phase structure with good surface coverage. The absorbance spectra of the film showed a broad range of absorbance from 400 to 760 nm suggesting that perovskite film has good absorption in visible reason. Fig. S1 (d) shows the morphology of pinhole free compact TiO_2 film.

3.1 Structural, morphological and optical characteristics of Ta-doped TiO_2 films

Fig. 1 (a) shows the XRD patterns of pristine TiO_2 and Ta-TiO_2 films having different mol% of Ta. It can be deduced from the figure that all the samples possess anatase phase (ICDD file No. 01-084-1285). No peak for elemental Ta or Ta_2O_5 could be detected in the XRD plots, suggesting that Ta is doped uniformly in crystal lattice of TiO_2. Due to lower effective mass of electron in anatase phase, anatase TiO_2 shows higher electrical conductivity as compared to rutile phase and hence is the desirable phase. However, there is also significant peak broadening upon Ta doping as intensity of (101) reflection as well as of other peaks decreases with the increase in Ta doping and the peaks shift towards the smaller 2θ as shown in Fig. 1 (b). Latter is because the ionic radius of Ta^{5+} (0.64 Å) is greater than the Ti^{4+} (0.61Å).[33] As suggested by the morphological studies (shown later), the peak broadening is not associated with the decrease in the grain size and hence it could perhaps be related to decreased crystallinity of the films overall.

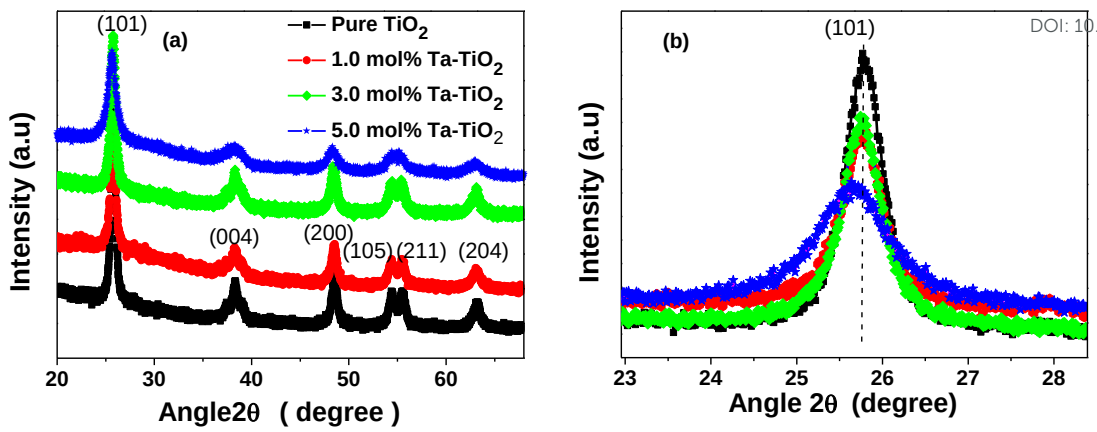

Fig. 1 XRD patterns of (a) pristine TiO_2 and various Ta-doped TiO_2 and (b) magnified spectra of (101) anatase crystal plane.

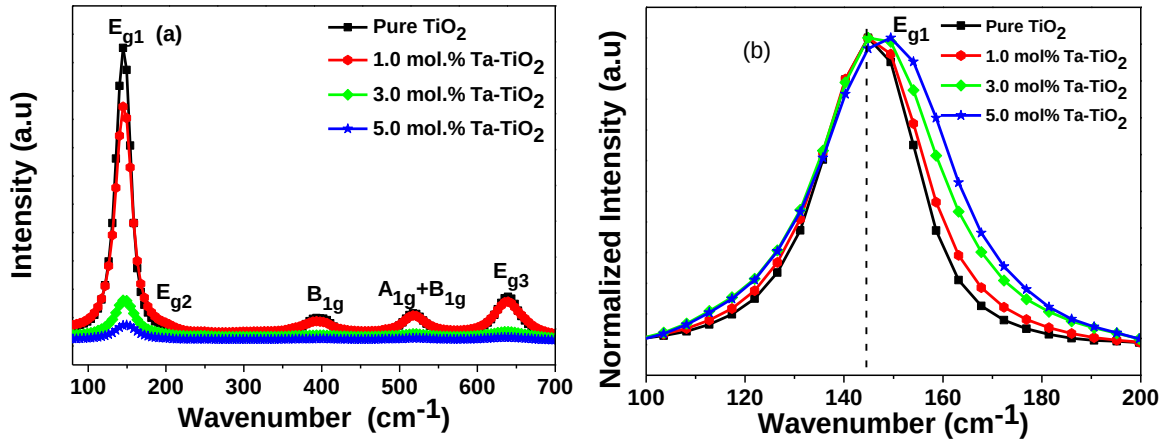

Fig. 2 Raman spectra of (a) pristine TiO_2 and various Ta-doped TiO_2 samples and (b) Normalized E_{g1} vibration Raman peak.

While XRD data provided broad and average information over a large sampling volume, Raman spectra can provide information at much smaller length scales and is sensitive to the crystallinity. The Raman spectra of undoped TiO_2 and 1.0, 3.0 and 5.0 mol% of Ta doped samples are shown in Fig. 2 (a). The well assigned Raman peaks at 144, 397, 521 and 639 cm^{-1} are observed in all the samples. Theses peaks are attributed to the vibration modes of E_{g1}, B_{1g}, A_{1g}+ B_{1g} and E_{g3}, respectively and thus confirm the presence of anatase phase of TiO_2. The weak peak of anatase phase at 194 cm^{-1} of E_{g2} can also be noticed. In rutile phase, four Raman peaks are observed due to oxygen atom vibrations which do not involve Ti-atom. However, in anatase phase, six active Raman vibrations are observed. Thus, Raman spectra

View Article Online
DOI: 10.1039/C7TA09193A

confirm the presence of anatase phase in compact TiO_2 layer, which is in agreement with XRD results. Further, except B_{1g} which shows only Ti-atom vibration, all others are mixture of both O-atom and Ti-atom motions in the anatase phase.[34] Fig. 2 (b) shows the normalized E_{g1} anatase vibration signal of the pure TiO_2 and doped samples. The Raman shift as well as the increment of full width half maxima (FWHM) is observed in the doped films. The E_g peak in Raman Spectra represents the symmetric stretching vibration of O-Ti-O in TiO_2. If doping occurs at substitutional position on the Ti^{4+}, the Ti-O-Ti bond gets disturbed and new Ta-O-Ti or Ta-O-Ta bonds form. The Raman active mode is affected due to this new Ta-O bond which formed in place of Ti-O bond and results in shifting and widening of peaks.[35] Thus, both Raman shift to higher wave number and widening of peaks suggest towards incorporation of Ta doping in the TiO_2 layer.[29]

The absorption spectra of pristine TiO_2 and various Ta-doped in TiO_2 films are shown in Fig. 3(a). The absorption spectra of doped thin films show red shift upon Ta doping as suggested by the band gap calculations of pure TiO_2 and doped TiO_2 thin films, calculated using Tauc plots (Fig. 3 (b)). The band gap of various tantalum doped compact TiO_2 films decreased with the increase of Ta doping percentage. The calculated value for pristine TiO_2 was 3.59 eV and remains nearly the same for 1.0 % Ta-TiO_2 film at ~3.58 eV. At increased doping levels, band gap decreased from 3.55 eV (3.0 mol% Ta-TiO_2) and 3.47 eV (5.0 mol% Ta-TiO_2), in agreement with the previously reported values. [36]

View Article Online
DOI: 10.1039/C7TA09193A

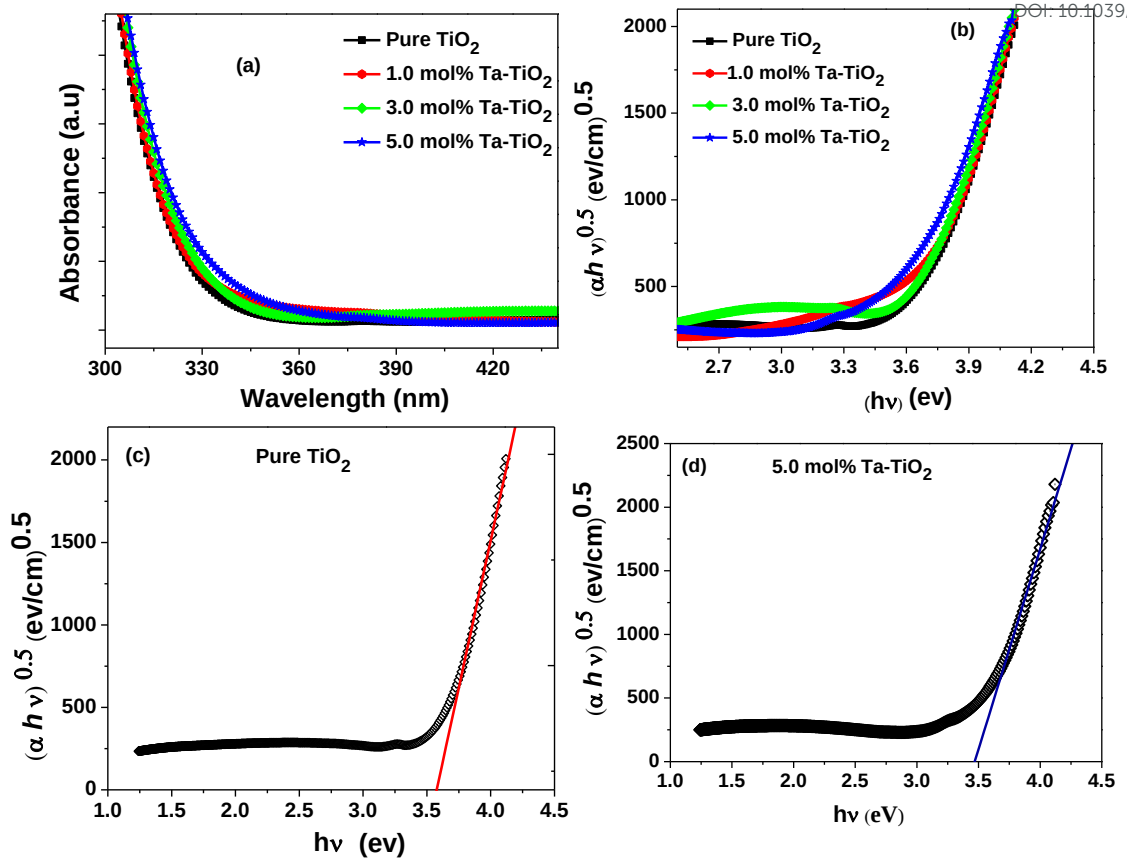

Fig. 3 (a) The UV-Vis absorption spectra of pristine and various Ta doped thin films (b) corresponding Tauc plot, (c) and (d) the band gap calculation using Tauc plot of pristine TiO_2 and 5.0 mol.% Ta doped thin film.

The interface between the active layer and the bottom electrode has an important effect on the device performance. Therefore, it is critical to examine the roughness of TiO_2 layer**.** Fig. 4 show AFM images for the surface of pure TiO_2 and tantalum doped thin films deposited on FTO coated glass substrate showing dense and compact grains in all the thin films. However, the RMS roughness of the film slightly increases from 11.3 nm (pure TiO_2) to 15.5 nm (5.0 mol.% Ta-TiO_2) upon increase in Ta doping.

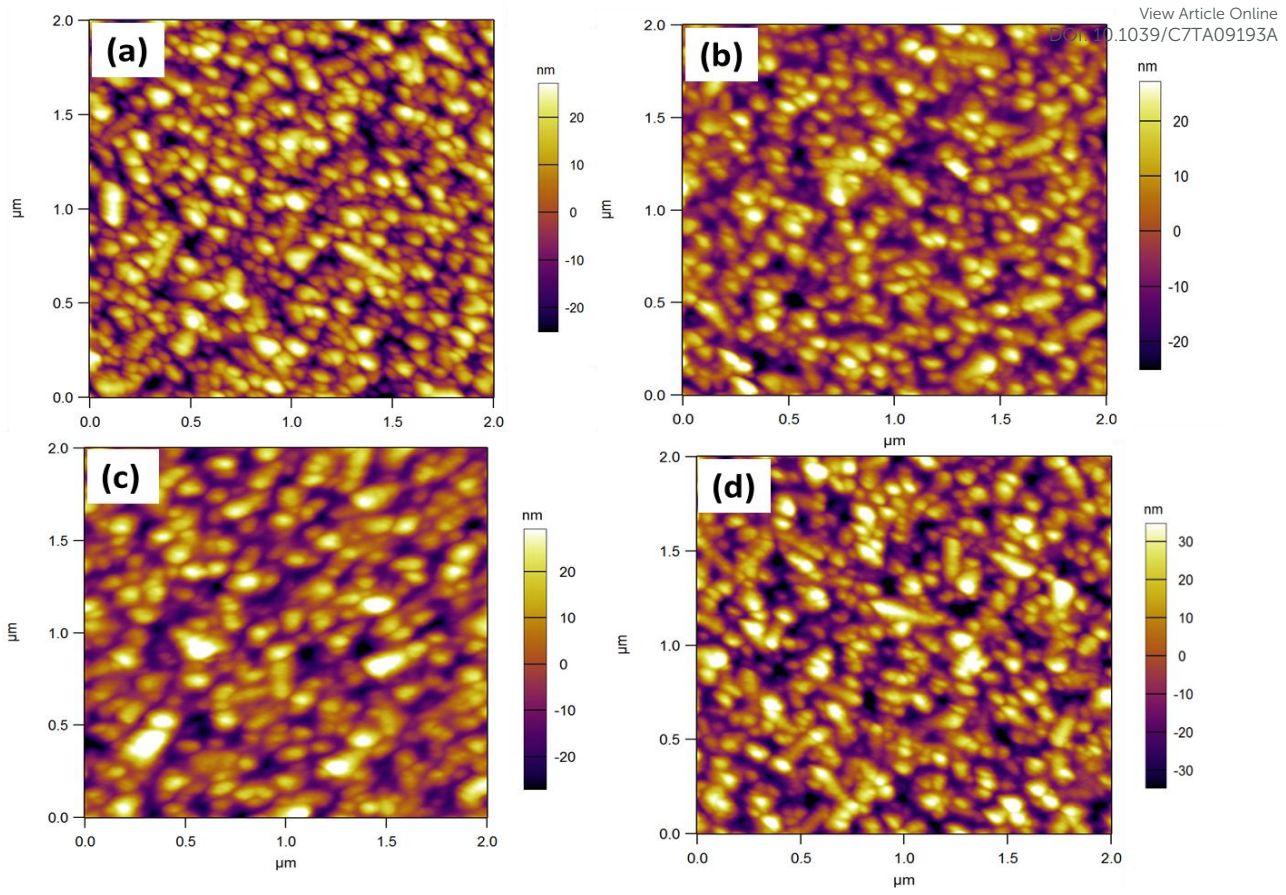

Fig. 4 AFM images of (a) pure TiO_2 (R_{RMS}:11.3 nm) (b) 1.0 mol.% Ta-TiO_2 (R_{RMS}: 11.6 nm) (c) 3.0 mol.% Ta-TiO_2 (R_{RMS}:12.6 nm) (d) 5.0 mol.% Ta-TiO_2 (R_{RMS}:15.5 nm) compact layer made on FTO coated glass substrate respectively (R_{RMS}: RMS roughness).

The surface roughness of tantalum doped TiO_2 compact layer could play a significant role in electron transport as it affects the contact area between the perovskite active layers and Ta doped TiO_2 compact layer. Higher roughness could lead to an increase in the contact area between active layer and the electron transport layer leading to improved charge transportation.[37-38] However, doping level beyond 3.0% results in other problems such as formation of voids even though 5.0% Ta-TiO_2 films show highest r.m.s. roughness, resulting in lower conductivity as well as poor charge extraction as compared to 3.0 mol% doped thin films as shown in subsequent sections.

To confirm the tantalum doping in the TiO_2 thin films, XPS analysis was performed to study the electronic structure and chemical changes due to Ta doping. Fig. 5 (a) shows the full XPS spectra of pure TiO_2 and tantalum doped TiO_2 thin films. The obtained spectra illustrate that the pure TiO_2 film shows the presence of only Ti and O peaks whereas the doped thin films spectra consist of peaks from Ti, O and Ta elements. Fig. 5 (b) shows the characteristics

View Article Online
DOI: 10.1039/C7TA09193A

binding energy peaks of Ta 4f at 26.4 eV and 28.3 eV for $4f_{7/2}$ and $4f_{5/2}$, respectively. Increase in Ta amount is observed for 5.0 mol% Ta-TiO_2 compared to 3.0 mol% Ta-TiO_2 sample while Ta is absent in the pristine TiO_2 sample (Fig. 5c). The presence of Ta^{5+} in the doped thin film confirms the doping of Ta in pristine TiO_2 thin film.[25, 39-40] Table S1 contains atomic % of various elements for undoped TiO_2 and Ta-TiO_2 thin film samples which shows that Ta content increases with increase in the Ta doping. The high resolution XPS spectrum of Ti in undoped TiO_2 sample shows $2p_{3/2}$ and $2p_{1/2}$ characteristic peaks at binding energies of 459.1 eV and 464.8 eV, respectively corresponding to Ti^{4+} oxidation state (Fig. 5d). However, a detectable peak at lower binding energy is observed than the peak appeared at 459 eV for 3.0 mol% Ta-TiO_2 sample (Fig. 5e). This additional peak at 457 eV appears after the Ta doping which refers to Ti^{3+} oxidation state due to incorporation of Ta^{5+} ions within the crystal structure.[41-43]

View Article Online
DOI: 10.1039/C7TA09193A

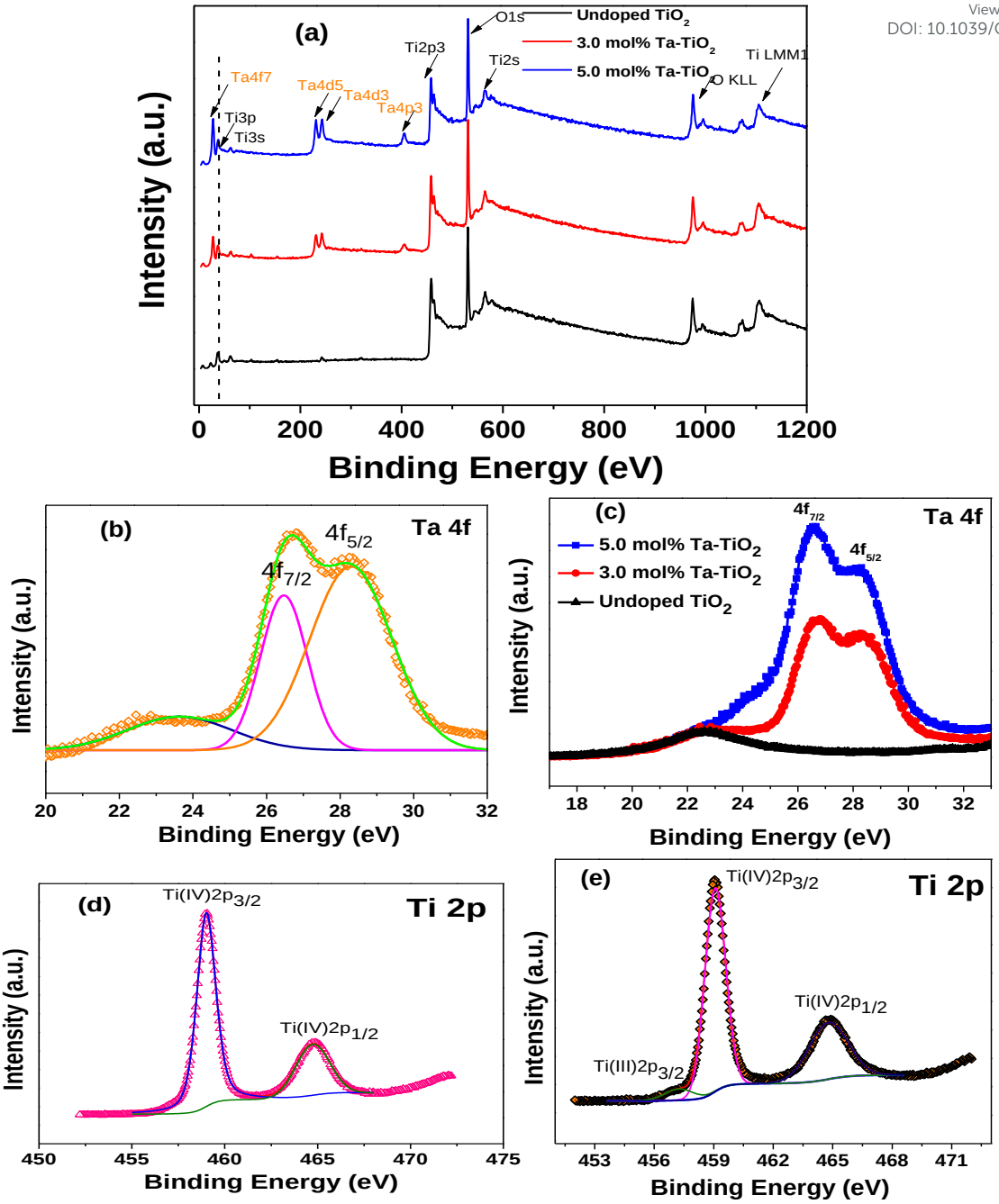

Fig. 5 (a) XPS spectra of undoped TiO_2, 3.0 mol.% Ta-TiO_2 and 5.0 mol% Ta-TiO_2 thin films prepared on FTO glass substrate; Ta_{4f} spectra for (b) 3.0 mol.% Ta-TiO_2 and (c) undoped TiO_2, 3.0 mol.% Ta-TiO_2 and 5.0 mol% Ta-TiO_2; Ti_{2p} spectra for (d) undoped TiO_2 and (e) 3.0 mol% Ta-TiO_2.

View Article Online
DOI: 10.1039/C7TA09193A

To find out the role of Ta doping on TiO_2 work function, which could have influence on the migration of electrons to the cathode, we conducted Kelvin probe force microscopy (KPFM) of the undoped and 3.0 mol% Ta-TiO_2 film. KPFM is an atomic force microscopy technique which measures the distributed contact potential difference (CPD) between the tip and the sample, through equation 1, which can be used to assess the surface potential.[44]

$$V_{CPD} = \frac{\varphi_{tip} - \varphi_{sample}}{e} \qquad (1)$$

Here, *e* is the electronic charge and ϕ_{tip} and ϕ_{sample} are the work functions of the tip and the sample, respectively. The scanned area of 5 µm× 5 µm was taken for KPFM imaging. As the Fig. 6 shows, the Ta-doped TiO_2 film showed the CPD value of -39 mV in comparison to undoped TiO_2 film having CPD value of 89 mV. Thus decrease of ~128 mV of CPD could be manifested in the shift of Fermi level of doped film. The ϕ_{tip} has value of 5.0 eV, thus the Fermi level of sample can be calculated as $\Phi_{sample} = \Phi_{tip} - eV_{CPD}$.[45] The calculated value for undoped film was 4.9 eV. For 3.0% Ta-TiO_2, the value was 5.04 eV. The lower edge of conduction band (CB) in TiO_2 consists of Ti^{4+} 3d bands and upper edge of valance band (VB) is made of O^{2-} 2p bands. As it is known that *n*- or *p*-type dopant affects the CB or VB of material but due to defect ridden nature in TiO_2, the doping affect the trap states. The doping can either decrease the deep trap density which can shifts the CB and Fermi level upward. In this case, V_{oc} increased but J_{sc} decreased due to decrease in driving force for electron injection. When doping contributes to the formation of deep trap reverse trend is generally observed [46]. In our case, due to Ta doping the CB and Fermi level shift downward which is in agreement with the reports on Ta doped films in DSSC solar cell.[25] This change in the Fermi level can result in large gap between conduction band of TiO_2 and perovskite LUMO (Fig. 6(c)) which could improve electron injection as suggested by device characterization. [46]

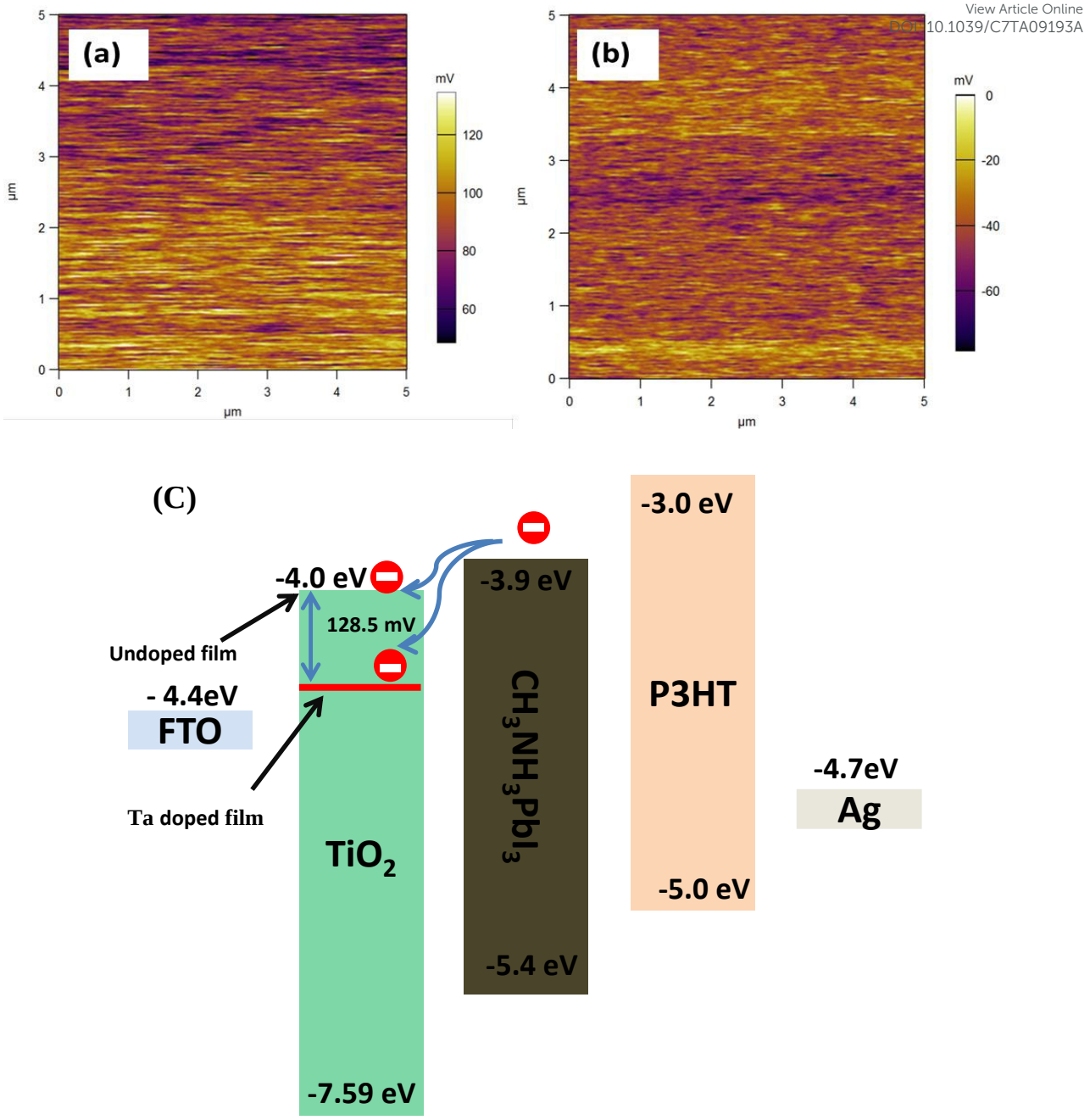

Fig. 6 KPFM image of (a) undoped TiO_2 film (b) 3.0 % mol Ta- TiO_2 film showing surface potential maps. (c) Schematic representation of energy band diagram of different layer.

View Article Online
DOI: 10.1039/C7TA09193A

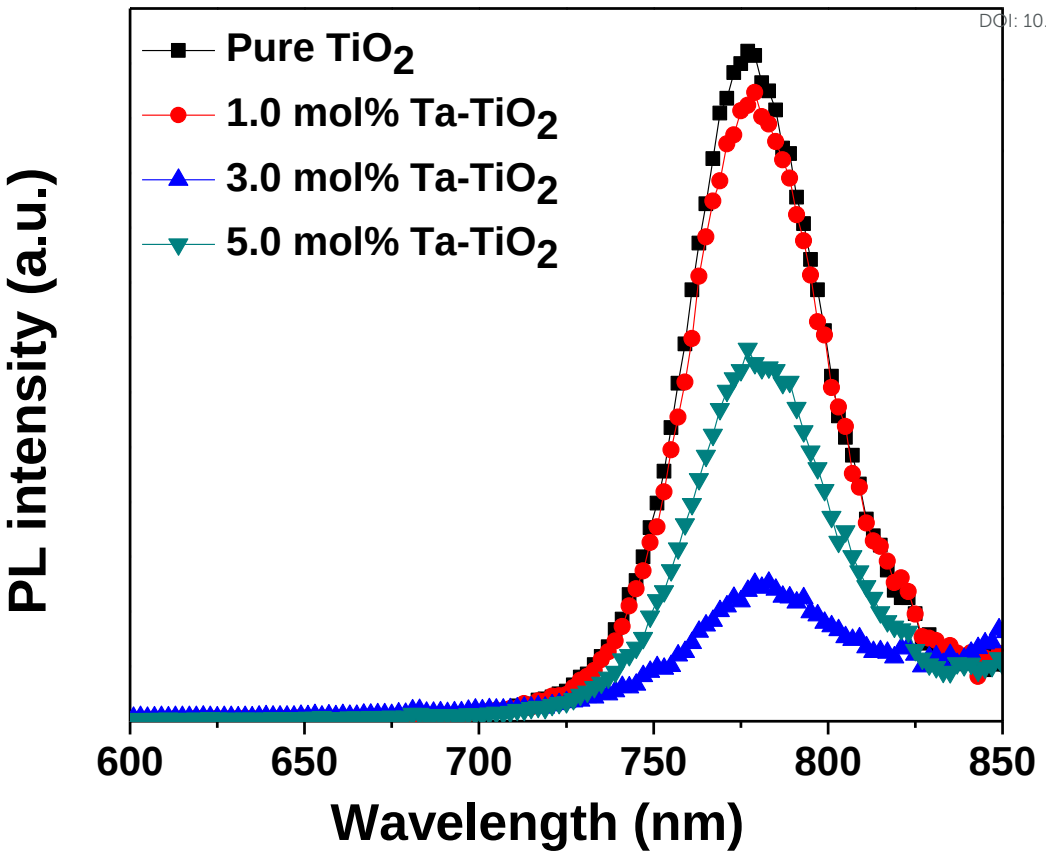

Fig.7 Photoluminescence (PL) spectra (excitation at 500 nm) of perovskite film on pristine TiO_2 and different mol% Ta-doped TiO_2 thin films.

Further to analyse whether the Ta-doped TiO_2 films affect the carrier recombination or extraction at the interface, we carried out the photoluminescence measurements on the doped and undoped TiO_2 films. Fig. 7 shows the steady state photoluminescence spectra of perovskite on pure TiO_2 and different mol% doped TiO_2 thin films deposited on FTO glass. From the Fig. it is clear that as we doped tantalum in TiO_2 film, photoluminescence of perovskite films gets quenched as evident from the decrease in the intensity of the PL peak with increasing Ta doping in TiO_2 thin films with 3.0 mol% Ta doped thin films showing maximum PL quenching due to the highest conductivity of the doped thin films. This suggests that Ta doping in pure TiO_2 films could be responsible for enhanced rate of photo-generated charge carrier extraction at the compact layer and perovskite interface.

3.2 Electrical Characterization of undoped and Ta-doped TiO_2 films

One of the effects of Ta doping on TiO_2 is to modify its electrical conductivity *via* promotion of anatase phase. To analyse this variation upon Ta doping into TiO_2 layer, we measured the current–voltage (*I*-V) characteristics of device structure FTO/Ta doped TiO_2 (0-5.0

mol.%)/Au and the results are shown in Fig. 8. The dc conductivity (σ_0) of the samples are calculated using the eqn 2

$$I = \sigma_0 A L^{-1} V \qquad (2)$$

where A (9.0 mm^2) is area of the devices and L (~ 68 nm) is the thickness of thin films. The conductivity of pure TiO_2 was measured from eqn 2 as 0.73 ± 0.13 x 10^{-3} mS/cm. With 1.0% Ta-TiO_2 the conductivity increased to 1.64 ± 0.1 x 10^{-3} mS/cm. For 3.0% doping the calculated conductivity was 3.29±0.18 x 10^{-3} mS/cm. The conductivity showed one order increment from pure TiO_2 (0.0 mol%) to 3.0 mol% Ta doping. However, at higher molar concentration (5.0 mol%), conductivity decreased to 2.68 ± 0.5 x 10^{-3} mS/cm. It may be due to formation of pinholes or higher roughness in the doped films.

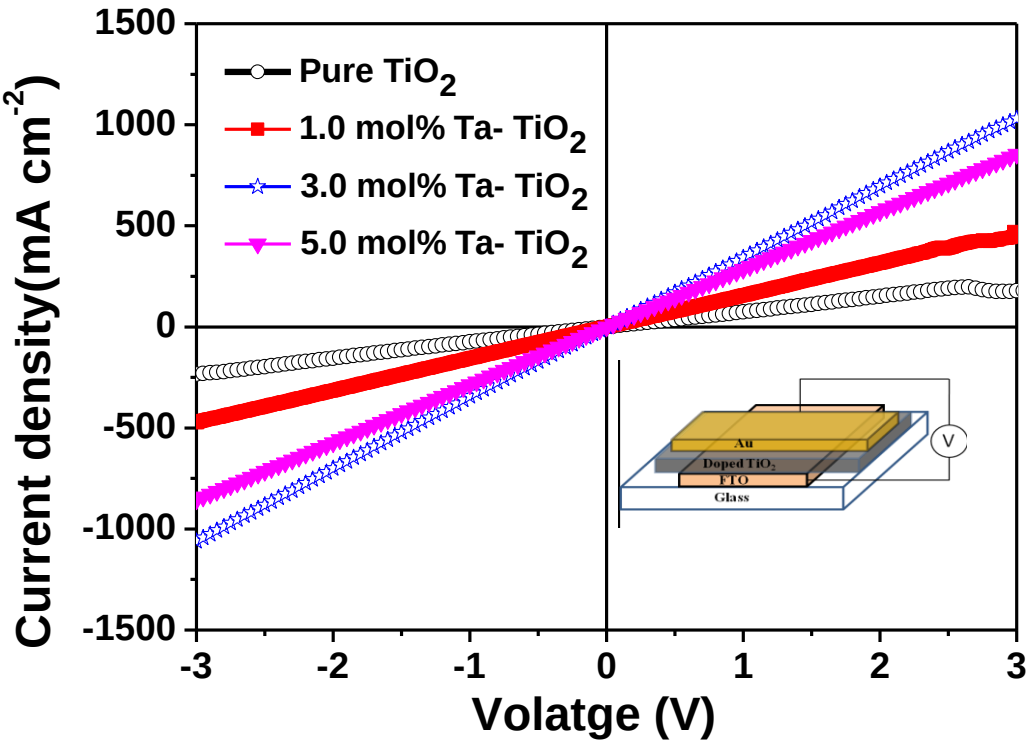

Fig. 8 Current density–voltage (*J-V*) characteristics of pristine and Ta doped TiO_2 thin films having device structure FTO/ Ta-TiO_2 doped (0-5 mol%)/Au. Inset shows the device structure.

View Article Online
DOI: 10.1039/C7TA09193A

3.3 Integration into Perovskite Solar Cells and Photovoltaic performance

The perovskite devices were fabricated using the device structure FTO/compact-TiO_2/$CH_3NH_3PbI_3$/P3HT/Ag, as shown in Fig. 9(a), where, TiO_2 layer was either in undoped or Ta-doped form. As the photovoltaic characteristics are shown Table 1, the average power conversion efficiency of the devices with un-doped TiO_2 film was 4.89% in the forward sweep direction with V_{oc} ~ 0.85 V, J_{sc} ~ 18.4 $mAcm^{-2}$, FF ~ 0.32. Generally, researchers have used Spiro-OMeTAD with Li-TFSI and tBP as dopant and $CH_3NH_3PbI_{3-x}Cl_x$ (*i.e.* mixture of methyl ammonium lead iodide and chloride) as active layer. Having incorporated mesoporous TiO_2 they have achieved high efficiency. In this device, we have used planar structure with no doping in P3HT which is the reason behind comparatively low efficiency of pristine device. However, the performance is comparable with literature where researchers have used P3HT as HTL having planar structure.[47] Further, poor fill factor is mainly attributed to higher series resistance, as both compact TiO_2 and undoped P3HT have low conductivity leading to high series resistance of 48 Ωcm^2. With the doping of 1.0 mol % Ta in compact TiO_2, due to increase in conductivity, series resistance decreases to 29 Ωcm^2, hence slight increase in J_{sc} can be noticed. But at the same time, V_{oc} decreases slightly from 0.85 V to 0.83 V which neutralises the enhancement in efficiency. With 3.0 mol % Ta-TiO_2 doping, the efficiency increase to 6.81% due to increase in J_{sc} (20.6 $mAcm^{-2}$) and FF (0.41) although there was again a little decrease in V_{oc} from 0.85 V to 0.83 V compared to undoped TiO_2. These trends can be explained by the fact that Ta doping causes the Fermi level as well as conduction band to shift downward. As V_{oc} is defined as the difference between the Fermi level of TiO_2 and HTM, shifting of Fermi level leads to a decreased V_{oc}, as also suggested by KPFM image in Fig. 6. However, at the same time due to larger difference between perovskite LUMO and TiO_2 conduction band, electron injection and hence J_{sc} increases.[46] These observations are in agreement with the previous data on DSSC solar cells using Ta doped TiO_2.[39] In our case, the best device was with 3.0 % tantalum doping which exhibited a PCE of 9.24% with J_{sc} of 21.13 $mAcm^{-2}$, V_{oc} of 0.90 and FF of 0.49. For 5.0 mol% Ta doping, V_{oc} further decreases to 0.75 as explained above and efficiency decreases. We also observe a decrease in the shunt resistance and increase in series resistance for 5.0% doping, which can be correlated to the increase of roughness and voids in the film.[48]

The change in PCE and J_{sc} upon Ta doping of TiO_2 are also in agreement with the changes in external quantum efficiency (EQE) characteristics, as shown in Fig. 9(b) where 3.0 mol% Ta-TiO_2 devices show the best external quantum efficiency. Fig. 9(c), 9(d) shows the J-V curve

View Article Online
DOI: 10.1039/C7TA09193A

of undoped and doped (1.0-5.0%) device in (a) forward and (b) reverse sweep direction, respectively. Similar trend in the performance was also evident in the reverse sweep direction. The undoped device show an average efficiency of 6.63% which increased to 8.17 % for 3.0 mol % Ta doped device (Table 1). It is interesting to note that Ta doping reduced the hysteresis in the J-V curves as forward and reverse sweeps J-V characteristics show low difference. Small amount of hysteresis at high doping concentrations may be due to ferroelectric hysteresis of perovskite material or defects at the surface of these materials.[49] The best device for 3.0 mole% in reverse sweep was 9.94% with FF of 0.57 and J_{sc} of 19.4 $mAcm^{-2}$. Table S2 summarizes PCE data from recent literature having planar device structure. The obtained efficiency for our devices is at par or more than the reported planar device structure having P3HT as HTL.

Fig. 10(a) shows the J-V curve of the best device in forward and reverse scan direction. Since 3.0 mol% Ta-TiO_2 device has shown the best performance, effect of Ta doping in TiO_2 on charge transport was further analysed by impedance spectroscopy (IS). It was carried out in dark with a bias of 0.6 V and 5 mV AC signal was applied within frequency range of 100 Hz to 100 kHz. Fig. 10(b) shows the Nyquist plots of undoped and 3.0 mol% Ta-TiO_2 device with the equivalent circuit (inset).[50] The circuit consists of series resistance (R_s), parallel recombination resistance (R_{rec}) and constant phase element (CPE). The ohmic resistance is represented by R_s whereas R_{rec} is associated with interface charge transport process. The non-ideal behaviour of capacitor is associated with CPE.[51] The CPE values are 0.97 and 0.95 for undoped and 3.0 % Ta doped samples, respectively indicating that the interface is not perfectly electrical.[51] For undoped device, R_s is 7.5 $\Omega.cm^2$ whereas for the doped device, R_s reduces to 2.1 $\Omega.cm^2$ due to higher conductivity of Ta doped film. Further, recombination resistance is also increased from 88.9 Ω cm^2 for undoped device to 223 Ω cm^2 for doped device. This clearly confirms the effect of Ta doping in reducing the recombination losses in the devices with Ta-doped TiO_2 films.

View Article Online
DOI: 10.1039/C7TA09193A

Table-1 Summary of average photovoltaic performance of undoped TiO_2 and different Ta-doped TiO_2 devices in forward and reverse sweep direction for 10 devices.

Ta doping mol%	J_{sc} (mA cm^{-2})	V_{oc} (V)	FF	η (%)	R_S (Ω cm^2)	R_{SH} (Ω cm^2)
Forward sweep direction						
Pure TiO_2	18.40 ± 1.5	0.85 ± 0.05	0.32 ± 0.04	4.89 ± 0.83	48.3 ± 19.3	108.1 ± 33.6
1.0 mol%	18.93 ± 2.7	0.83 ± 0.04	0.30 ± 0.04	4.80 ± 0.92	29.1 ± 2.70	105.2 ± 19.6
3.0 mol%	20.60 ± 1.7	0.83 ± 0.05	0.41 ± 0.05	6.81 ± 1.99	18.5 ± 2.80	220.0 ± 65.3
5.0 mol%	19.20 ± 2.1	0.75 ± 0.06	0.32 ± 0.07	4.50 ± 1.33	23.3 ± 1.50	150.2 ± 70.1
Reverse sweep direction						
Pure TiO_2	20.40 ± 1.4	0.91 ± 0.06	0.36 ± 0.04	6.63 ± 0.54	45.7 ± 28.0	164.0 ± 44.8
1.0 mol%	22.60 ± 1.2	0.85 ± 0.03	0.35 ± 0.05	6.40 ± 0.47	25.6 ± 3.1	131.3 ± 32.7
3.0 mol%	22.10 ± 1.2	0.85 ± 0.04	0.42 ± 0.04	8.17 ± 0.97	17.4 ± 2.3	276.6 ± 81.6
5.0 mol%	21.60 ± 2.6	0.80 ± 0.05	0.37 ± 0.07	6.24 ± 0.76	19.6 ± 1.4	229.2 ± 30.3

View Article Online
DOI: 10.1039/C7TA09193A

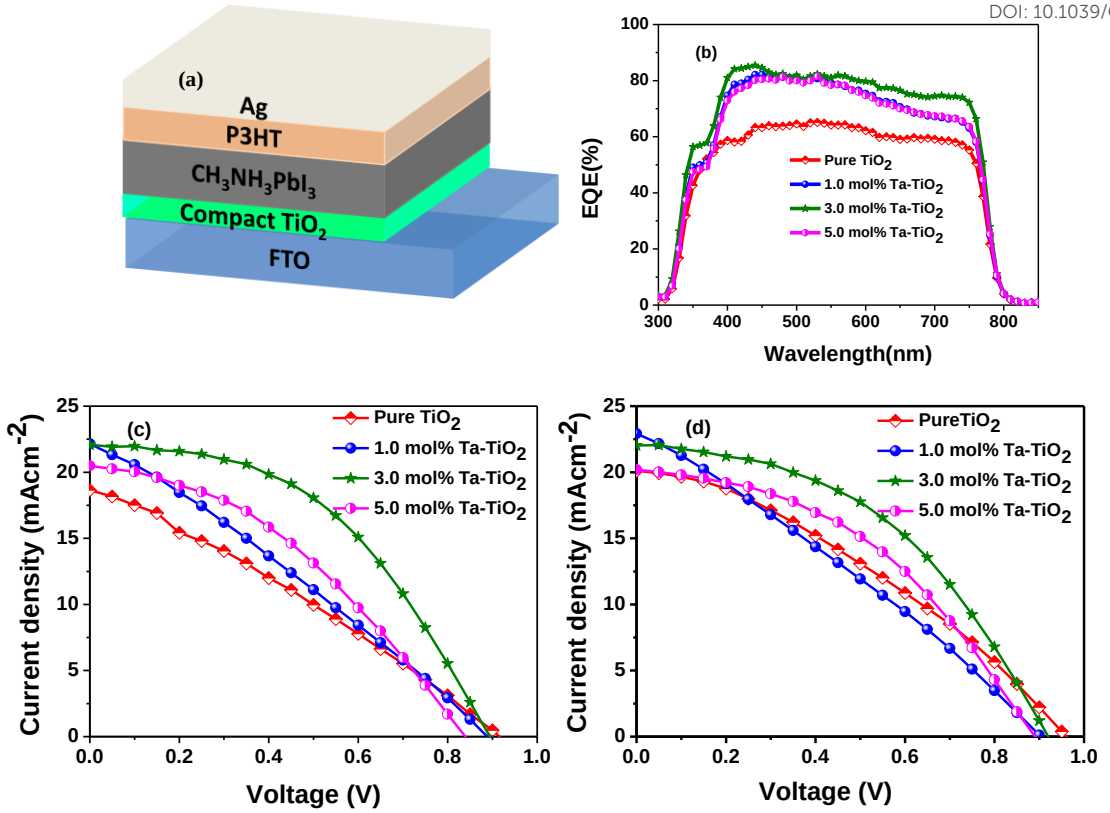

Fig. 9 (a) Schematic of planar conventional perovskite solar cell, (b) EQE of undoped and Ta (1.0-5.0%) doped device, J-V curve of undoped and doped (1.0-5.0 %) device in (c) forward and (d) reverse sweep direction.

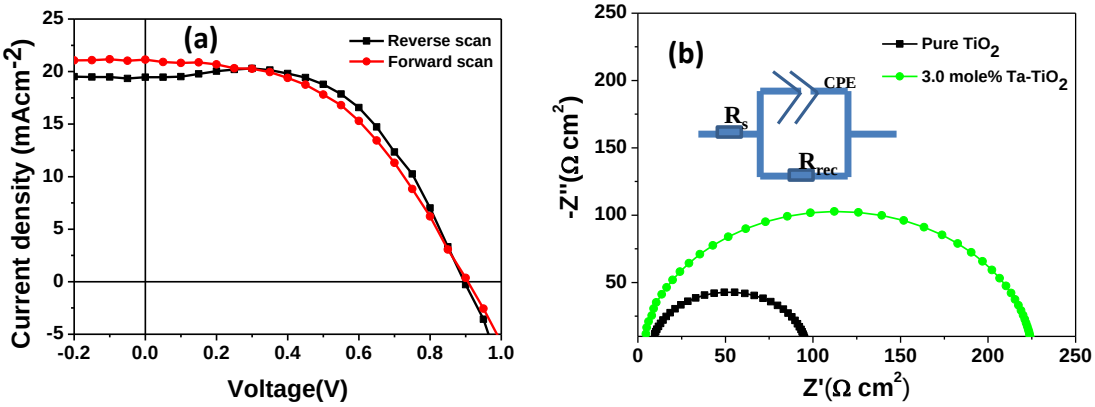

Fig. 10 (a) J-V curve of best device in forward and reverse sweep direction, (b) Nyquist plots of undoped and 3.0 mol% Ta-TiO_2 device in dark. Inset shows the equivalent circuit of Nyquist plot.

View Article Online
DOI: 10.1039/C7TA09193A

4. Conclusions

In summary, we have demonstrated the positive effect of Ta doping in compact TiO_2 layer resulting in substantial improvement in the device performance in Spiro-OMeTAD free planar perovskite solar cells. Quenching of photoluminescence upon Ta doping suggests that the electrons could be extracted more efficiently from perovskite film compared to undoped TiO_2 film. These effects resulted in an enhancement in FF due to lower series resistance and higher shunt resistance in the devices. The device showed improved J_{sc} due to lowering of Fermi level of TiO_2 shifted upon Ta doping and hence a larger gap between conduction band and perovskite LUMO provides a greater driving force for electron transfer. Thus, enhancement in current density was observed with Ta doping. The best device was achieved for 3.0 mol% Ta doping of TiO_2 with enhancement in efficiency to 9.24% in forward scan direction and 9.94% in reverse scan direction showing substantial improvement over device with undoped TiO_2.

ASSOCIATED CONTENT

Supporting Information

XRD pattern, absorbance data and morphology of the perovskite film, morphology of compact TiO_2 film. This material is available free of charge.

AUTHOR INFORMATION

Corresponding Author

*E-mail: guptark@iitk.ac.in

Notes

The authors declare no competing financial interest.

Acknowledgements

We acknowledge the financial support from DST-RCUK Grant no SR/RC-UK/APEX Phase II/2015 and DST Grant No. DST/TMD/CERI/C140(G) under Clean Energy Research Initiative. RKG acknowledges financial assistance from Department of Science and Technology (DST), India, through the INSPIRE Faculty Award (Project No. IFA-13 ENG-57). DST support to the Center for Nanosciences is acknowledged.

References

1. C. C. Stoumpos, C. D. Malliakas and M. G. Kanatzidis, *Inorg Chem*, 2013, **52**, 9019-9038.

2. Q. Dong, Y. Fang, Y. Shao, P. Mulligan, J. Qiu, L. Cao and J. Huang, *Science*, 2015, **347**, 967-970.

3. S. D. Stranks, G. E. Eperon, G. Grancini, C. Menelaou, M. J. P. Alcocer, T. Leijtens, L. M. Herz, A. Petrozza and H. J. Snaith, *Science*, 2013, **342**, 341-344.

4. G. Xing, N. Mathews, S. Sun, S. S. Lim, Y. M. Lam, M. Grätzel, S. Mhaisalkar and T. C. Sum, *Science*, 2013, **342**, 344-347.

5. N. Pellet, P. Gao, G. Gregori, T.-Y. Yang, M. K. Nazeeruddin, J. Maier and M. Grätzel, *Angew. Chem. Int. Ed.*, 2014, **53**, 3151-3157.

6. J. H. Noh, S. H. Im, J. H. Heo, T. N. Mandal and S. I. Seok, *Nano Lett.*, 2013, **13**, 1764-1769.

7. A. Kojima, K. Teshima, Y. Shirai and T. Miyasaka, *JACS*, 2009, **131**, 6050-6051.

8. W. S. Yang, B.-W. Park, E. H. Jung, N. J. Jeon, Y. C. Kim, D. U. Lee, S. S. Shin, J. Seo, E. K. Kim, J. H. Noh and S. I. Seok, *Science*, 2017, **356**, 1376-1379.

9. M. Saliba, T. Matsui, J.-Y. Seo, K. Domanski, J.-P. Correa-Baena, M. K. Nazeeruddin, S. M. Zakeeruddin, W. Tress, A. Abate, A. Hagfeldt and M. Gratzel, *Energy Environ Sci.*, 2016, **9**, 1989-1997.

10. H. Yoon, S. M. Kang, J.-K. Lee and M. Choi, *Energy Environ Sci.*, 2016, **9**, 2262-2266.

11. J. Yang, B. D. Siempelkamp, D. Liu and T. L. Kelly, *ACS Nano*, 2015, **9**, 1955-1963.

12. M. Liu, M. B. Johnston and H. J. Snaith, *Nature*, 2013, **501**, 395-398.

13. K. Mahmood, S. Sarwar and M. T. Mehran, *RSC Advances*, 2017, **7**, 17044-17062.

14. D. Liu and T. L. Kelly, *Nature Photonics*, 2013, **8**, 133.

15. Z.-L. Tseng, C.-H. Chiang and C.-G. Wu, *Scientific Reports*, 2015, **5**, 13211.

16. L. Kavan, L. Steier and M. Grätzel, *J. Phys. Chem. C*, 2017, **121**, 342-350.

17. L. Kavan, *Journal of Solid State Electrochemistry*, 2014, **18**, 2297-2306.

18. M. Khan and W. Cao, *Journal of Molecular Catalysis A: Chemical*, 2013, **376**, 71-77.

19. H. Zhou, Q. Chen, G. Li, S. Luo, T.-b. Song, H.-S. Duan, Z. Hong, J. You, Y. Liu and Y. Yang, *Science*, 2014, **345**, 542-546.

20. J. H. Heo, M. S. You, M. H. Chang, W. Yin, T. K. Ahn, S.-J. Lee, S.-J. Sung, D. H. Kim and S. H. Im, *Nano Energy*, 2015, **15**, 530-539.

21. B.-X. Chen, H.-S. Rao, W.-G. Li, Y.-F. Xu, H.-Y. Chen, D.-B. Kuang and C.-Y. Su, *J. Mater. Chem. A*, 2016, **4**, 5647-5653.

22. J. Wang, M. Qin, H. Tao, W. Ke, Z. Chen, J. Wan, P. Qin, L. Xiong, H. Lei, H. Yu and G. Fang, *Appl. Phys. Lett.*, 2015, **106**, 121104.

23. M.-C. Wu, S.-H. Chan, M.-H. Jao and W.-F. Su, *Sol. Energ. Mat. Sol. Cells*, 2016, **157**, 447-453.

24. X.-X. Gao, Q.-Q. Ge, D.-J. Xue, J. Ding, J.-Y. Ma, Y.-X. Chen, B. Zhang, Y. Feng, L.-J. Wan and J.-S. Hu, *Nanoscale*, 2016, **8**, 16881-16885.

25. J. Liu, H. Yang, W. Tan, X. Zhou and Y. Lin, Electrochim. Acta, 2010, **56**, 396-400.

26. J.-H. Choi, S.-H. Kwon, Y.-K. Jeong, I. Kim and K.-H. Kim, *J. Electrochem. Soc.*, 2011, **158**, B749-B753.

27. D. Liu, S. Li, P. Zhang, Y. Wang, R. Zhang, H. Sarvari, F. Wang, J. Wu, Z. Wang and Z. D. Chen, *Nano Energy*, 2017, **31**, 462-468.

28. S. M. Bawaked, S. Sathasivam, D. S. Bhachu, N. Chadwick, A. Y. Obaid, S. Al-Thabaiti, S. N. Basahel, C. J. Carmalt and I. P. Parkin, *J. Mater. Chem. A*, 2014, **2**, 12849-12856.

29. Y. F. Zhao, C. Li, J. Y. Hu, Y. Y. Gong, L. Y. Niu and X. J. Liu, *Phys. Lett. A*, 2016, **380**, 910-916.

30. H. Krysova, P. Mazzolini, C. S. Casari, V. Russo, A. L. Bassi and L. Kavan, Electrochim. Acta, 2017, **232**, 44-53.

31. L. Kavan, N. Tétreault, T. Moehl and M. Grätzel, *J. Phys. Chem. C*, 2014, **118**, 16408-16418.

32. M. M. Lee, J. Teuscher, T. Miyasaka, T. N. Murakami and H. J. Snaith, *Science*, 2012, **338**, 643-647.

33. R. M. Pasquarelli, D. S. Ginley and R. O'Hayre, *Chem. Soc. Rev.*, 2011, **40**, 5406-5441.

34. O. Frank, M. Zukalova, B. Laskova, J. Kurti, J. Koltai and L. Kavan, *Physical Chemistry Chemical Physics*, 2012, **14**, 14567-14572.

35. B. Choudhury, M. Dey and A. Choudhury, *Int Nano Lett*, 2013, **3**, 25.

36. A. Nakaruk, D. Ragazzon and C. C. Sorrell, *Thin Solid Films*, 2010, **518**, 3735-3742.

37. Z. Jehl, M. Bouttemy, D. Lincot, J. F. Guillemoles, I. Gerard, A. Etcheberry, G. Voorwinden, M. Powalla and N. Naghavi, *J. Appl. Phys.*, 2012, **111**, 114509.

38. M.-H. Hsu, P. Yu, J.-H. Huang, C.-H. Chang, C.-W. Wu, Y.-C. Cheng and C.-W. Chu, *Appl. Phys. Lett.*, 2011, **98**, 073308.

39. R. Ghosh, Y. Hara, L. Alibabaei, K. Hanson, S. Rangan, R. Bartynski, T. J. Meyer and R. Lopez, *ACS Appl. Mater. Interfaces*, 2012, **4**, 4566-4570.

40. P. Xiang, W. Ma, T. Xiao, L. Jiang, X. Tan and T. Shu, *J. Alloys Compd.*, 2016, **656**, 45-50.

41. Y. Gao, S. Thevuthasan, D. E. McCready and M. Engelhard, *J. Cryst. Growth*, 2000, **212**, 178-190.

42. B. Gong, X. Luo, N. Bao, J. Ding, S. Li and J. Yi, *Surf. Interface Anal.*, 2014, **46**, 1043-1046.

43. L. R. Sheppard, S. Hager, J. Holik, R. Liu, S. Macartney and R. Wuhrer, *J. Phys. Chem. C*, 2015, **119**, 392-400.

44. S. K. Gupta, R. Jindal and A. Garg, *ACS Appl. Mater. Interfaces*, 2015, **7**, 16418-16427.

45. T. Su and H. Zhang, *PLoS ONE*, 2017, **12**, e0171050.

46. B. Roose, S. Pathak and U. Steiner, *Chem. Soc. Rev.*, 2015, **44**, 8326-8349.

47. W. Wang, H. Zheng, Y. Liu, J. Sun and L. Gao, *J. Nanosci. Nanotechnol.*, 2016, **16**, 12768-12772.

48. D. Liu, M. K. Gangishetty and T. L. Kelly, *J. Mater. Chem. A*, 2014, **2**, 19873-19881.

49. H. J. Snaith, A. Abate, J. M. Ball, G. E. Eperon, T. Leijtens, N. K. Noel, S. D. Stranks, J. T.-W. Wang, K. Wojciechowski and W. Zhang, *J. Phys. Chem. Lett.*, 2014, **5**, 1511-1515.

50. M. Hu, L. Liu, A. Mei, Y. Yang, T. Liu and H. Han, *J. Mater. Chem. A*, 2014, **2**, 17115-17121.

51. W. Liu and Y. Zhang, *J. Mater. Chem. A*, 2014, **2**, 10244-10249.

View Article Online
DOI: 10.1039/C7TA09193A

TOC

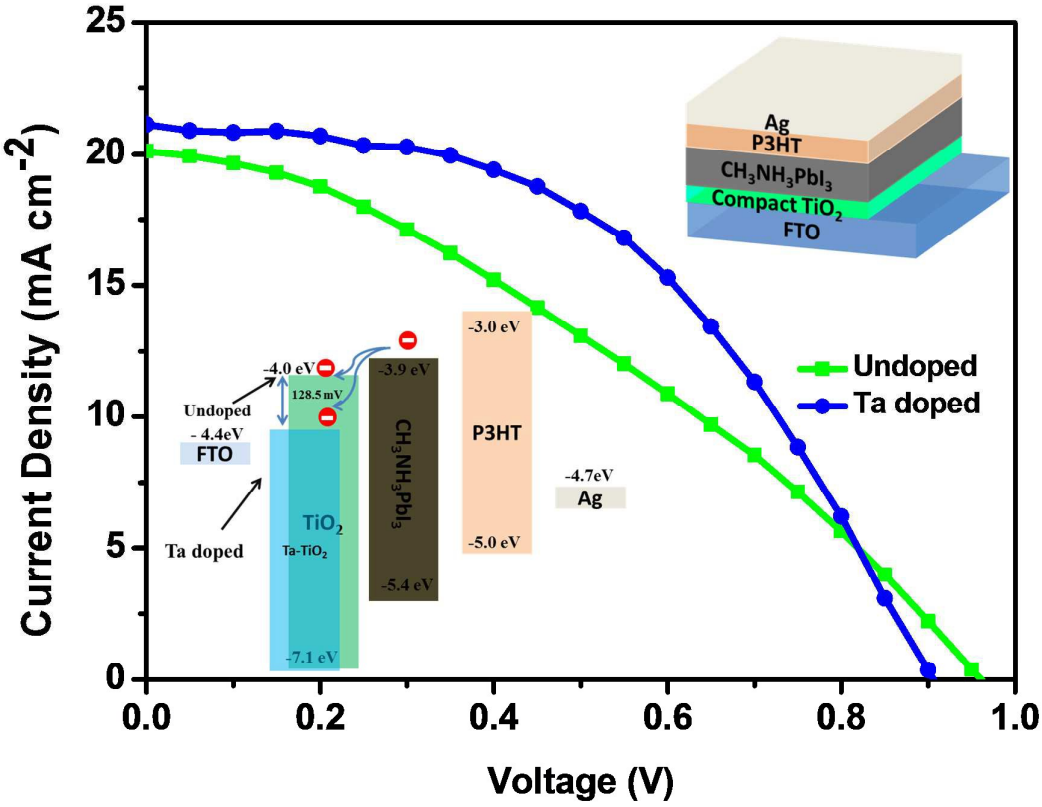

This work investigates the effect of tantalum doping in compact TiO_2 layer on the performance of planar Spiro-OMeTAD free perovskite solar cells. 40% improvement in the overall efficiency was obtained as compared to the device with undoped TiO_2.